Available online at http://onlinelibrary.wiley.com/doi/10.1111/maps.12462/abstract

DOI: 10.1111/maps.12462

Identification of Magnetite in Lunar Regolith Breccia 60016: evidence for oxidised conditions at the lunar surface

Katherine H. Joy[1,2,3], Channon Visscher[4], Michael E. Zolensky[5], Takashi Mikouchi[6], Kenji Hagiya[7], Kazumasa Ohsumi[8], and David A. Kring[1,2]

[1]Center for Lunar Science and Exploration, The Lunar and Planetary Institute - USRA, 3600 Bay Area Blvd., Houston, Texas 77058, USA.

[2]NASA Lunar Science Institute.

[3]now based at School of Earth, Atmospheric and Environmental Sciences, University of Manchester, Oxford Road, Manchester, M13 9PL, UK.

[3]Dordt College 498, 4th Avenue NE Sioux Center, Iowa 51250-1606, USA.

[5]ARES, NASA Johnson Space Center, Houston, TX 77058, USA.

[6]Department of Earth and Planetary Science, Graduate School of Science, University of Tokyo, 7-3-1, Hongo, Bunkyo-ku, Tokyo, 113-0033, Japan.

[7]Graduate School of Science, University of Hyogo, 3-2-1 Koto, Kamigori, Ako-gun, Hyogo 678-1297, Japan.

[8]Japan Synchrotron Radiation Research Institute (JASRI), 1-1-1 Koto, Sayo-cho, Sayo-gun, Hyogo 679-5198, Japan

Corresponding author email: katherine.joy@manchester.ac.uk

Key words: lunar-regolith, regolith-breccia, magnetite, lunar-volatiles, lunar-oxidation

Proposed running header: Magnetite in Lunar Regolith Breccia 60016

Abstract

Lunar regolith breccias are temporal archives of magmatic and impact bombardment processes on the Moon. Apollo 16 sample 60016 is an 'ancient' feldspathic regolith breccia that was converted from a soil to a rock at ~3.8 Ga. The breccia contains a small (70 × 50 µm) rock fragment composed dominantly of an Fe-oxide phase with disseminated domains of troilite. Fragments of plagioclase (An_{95-97}), pyroxene (En_{74-75}, Fs_{21-22},Wo_{3-4}) and olivine (Fo_{66-67}) are distributed in and adjacent to the Fe-oxide. The silicate minerals have lunar compositions that are similar to anorthosites. Mineral chemistry, synchrotron X-ray Absorption Near Edge Spectroscopy (XANES) and X-ray Diffraction (XRD) studies demonstrate that the oxide phase is magnetite with an estimated $Fe^{3+}/\Sigma Fe$ ratio of ~0.45. The presence of magnetite in 60016 indicates that oxygen fugacity during formation was equilibrated at, or above, the Fe-magnetite or wűstite-magnetite oxygen buffer. This discovery provides direct evidence for oxidised conditions on the Moon. Thermodynamic modelling shows that magnetite could have been formed from oxidisation-driven mineral replacement of Fe-metal or desulphurisation from Fe-sulphides (troilite) at low temperatures (<570 °C) in equilibrium with H_2O steam/liquid or CO_2 gas. Oxidising conditions may have arisen from vapour transport during degassing of a magmatic source region, or from a hybrid endogenic-exogenic process when gases were released during an impacting asteroid or comet impact.

1. Background

The lunar regolith is a boundary layer between endogenous lunar processes and the space environment (see Hörz et al., 1991; McKay et al., 1991 and Lucey et al., 2006 for detailed lunar reviews). It is formed of comminuted lunar rocks and mineral fragments, and has an added exogenous component from asteroids, comets and interplanetary dust and an implanted solar wind addition. Regolith can be consolidated by impact thermal and shock pressure events into coherent rocks called regolith breccias.

When a breccia assembly event occurs, the rock and its components are 'closed' to addition of further material, and, therefore, these samples can be used as time capsules; preserving a record of regolith processes at different times in lunar history (McKay et al., 1986, 1989; Korotev, 1996; Spudis and Taylor, 2009; Crawford et al., 2010; Joy et al., 2011, 2012; Fagan et al., 2014).

Both the lunar surface regolith environment and interior are generally thought to be highly reduced with oxygen fugacity (fO_2) estimates ranging from +0.2 to -2.5 log units relative to the Fe-wűstite (IW) buffer (Wadhwa, 2008 and references therein). Evidence for low-fO_2 conditions is given by (i) the extremely low ferric (3^+) iron content of lunar samples, and the valence state of Eu in plagioclase (Drake, 1978; Karner et al., 2004) and Cr, Ti, V in mafic minerals (Sutton et al., 1993; Papike et al., 2005; Shearer et al., 2006; Karner et al., 2006); (ii) the widespread occurrence of Fe-metal and other reduced phases (*e.g.*, troilite, stoichiometric ilmenite, armalcolite, hapkeite), both as native phases in lunar basalts and volcanic pyroclastic glasses, and from meteoritic-added metal and sulphide components in impact melt breccias and crystalline impact melt; (iii) the lack of oxidised Fe mineral phases (*e.g.*, Jedweb et al. 1970; Fun-Dow et al., 1973; Housley et al., 1974); (iv) experimentally measured fO_2 values (Sato et al., 1978; Sato, 1979); and (v) similarities between observed lunar igneous rock textures and crystallisation sequences, and low-fO_2 petrology experiments (*e.g.*, Longhi, 1992 and references therein).

Fe in the Fe^{3+} valence state has also occasionally been reported in lunar soils and surficial impact condensates (*e.g.*, Griscom and Marquardt, 1972; Forester, 1973; Dikov et al., 2009; Yakovlev et al., 2009), suggesting that unusual, possibly localised, variable oxidation states occur on the Moon. Detection of magnetite (with a chemical formula of Fe_3O_4 or $FeO{\cdot}Fe_2O_3$ to denote the range in oxidation state between ferric (3^+) and ferrous (2^+) iron species) and hematite (Fe_2O_3) mineral species in lunar rocks and soils has also been inferred by a variety of techniques (including electron microprobe, Mőssbauer spectroscopy, RAMAN spectroscopy, magnetic susceptibility and electron spin resonance studies: *e.g.*, Ramdohr and El Goresey, 1970; Weeks et al., 1970, 1972; Kolopus et al., 1971; Runcorn et al. 1971; Weeks, 1972; Griscom and Ma-Quardt 1972; Forester, 1973; Bell et al., 1974; Pasieczna-Patkowska et al., 2008; Dabrowski et al., 2008; Shearer et al., 2014). However, these observations have typically lacked validation by multiple analytical techniques, and interpretations have been subsequently been dismissed (*e.g.*, Housley et al., 1974; Griscom, 1974) or can be shown to be ambiguous: for example, the observation of hematite by RAMAN spectroscopy is probably caused by the oxidation of lunar ilmenite

or nano-phase iron during the analysis process in the presence of terrestrial atmosphere (see Ling et al., 2011 and Shearer et al., 2014 for details). The only definitive presence of magnetite reported to date in Apollo samples is that found in carbonaceous chondrite Bench Crater found at the Apollo 12 landing site (McSween, 1976; Zolensky et al., 1996; Zolensky, 1997). Fe-oxidation has been observed where akaganeite (β-FeOOH) and goethite ($Fe^{3+}O(OH)$) are associated with rusting of metallic-Fe particles in Apollo samples (Agrell et al., 1972; Williams and Gibson, 1972; Taylor et al., 1974; Haggerty, 1978; Hunter and Taylor, 1981; Shearer et al., 2014). However, the origin of these oxyhydration products are poorly understood, with interpretations ranging from lunar *in situ* alteration or direct mineral deposition to terrestrial alteration/contamination (Taylor et al., 1974; Taylor and Burton, 1976; Shearer et al., 2014).

Here, we characterise an Fe-oxide-bearing lithic fragment in Apollo 16 regolith breccia 60016. We demonstrate using electron microprobe, XANES (X-ray Absorption Near Edge Spectroscopy) and synchrotron XRD (X-ray Diffraction) analysis that this phase is magnetite; the first time that $FeO.Fe_3O_4$ has been unambiguously identified in a lunar sample using multiple analytical techniques.

2. Materials and Methods

A 30 µm thick polished section 60016,83 was allocated by CAPTEM (Curation and Analysis Planning Team for Extraterrestrial Materials). The section had previously been studied by Simon et al. (1988) and Joy et al. (2012). We analysed the section using optical microscopy and identified a fragment using reflected light microscopy as bearing sulphide and Fe-oxide. We do not believe the Fe-oxide was produced by terrestrial contamination as there are many examples of Fe-metal grains scattered throughout the 60016,83 breccia matrix and in lithic clasts that have not been altered.

The section was X-ray mapped using the NASA Johnson Space Center (JSC) JEOL 6340f Field Emission Gun Scanning Electron Microscope (FEG-SEM) using a beam current of 30 nA and an accelerating voltage of 15 kV to derive 1 micron per pixel spatially resolved element distribution and concentration maps (Fig. 1). Mineral chemistry was derived using the JSC Cameca SX100 electron microprobe (EMP) with a 1 micron beam, a beam current of 20 nA and an accelerating voltage of 15 kV. On element peak counting times were 10 s for Na, 30 s for Mn and Co and 20 s for other elements. Well-characterised

natural mineral and pure metal standards were used to calibrate the EMP measurements. Four different FeO standards (Marjalahti olivine, pure magnetite, pure hematite, pure Fe-metal) were used to calibrate the Fe analysis. The Fe-oxide data reported here represent those internally standardised with the pure magnetite Fe-standard (Table 1). The 60016,83 silicate mineral data was standardised using the Marjalahti olivine Fe-standard (Table 2). The 60016,83 sulphide data were standardised using the pure Fe-metal standard (Table 2). After EMP analysis the carbon coat was removed, and the sample was analysed using the Japanese Spring-8 and High Energy Accelerator Research Organisation facilities (KEK).

XANES spectra at the Fe K-absorption edge were measured by using a synchrotron radiation source and a Si(Li)-solid state detector (SSD) at BL-4A, Photon Factory (PF), Institute of Material Structure Science (IMSS), High Energy Accelerator Research Organization (KEK), Tsukuba, Japan. The SR X-ray was monochromatised with a Si (111) double crystal monochromator. The microfocusing Kirkpatrick-Baez mirrors were used to focus an incident X-ray beam of about 5 × 6 μm in size at the specimen surface (Monkawa et al., 2006). An ionisation chamber was used to monitor the X-ray incidence irradiating a single crystal specimen and SSD was mounted at about 90 degrees to the incident beam within the photon polarisation plane. The XANES spectra at the Fe K-absorption edge were obtained in the fluorescence mode by scanning the incident X-ray energy from 7103 to 7153 eV at an interval of 0.13 eV. The incident X-ray energy was calibrated by setting the first inflection point of the Fe K-edge of a metallic Fe foil at 7111.08 eV (Wilke et al., 2001). The pre-edge peak, which is located about 15–20 eV below the main K-absorption edges, is sensitive to Fe valence states. Such pre-edge signal is related to the metal electronic transition from 1*s* to 3*d* and/or from 1*s* to 4*p*. This pre-edge position shifts toward higher energy with increasing $Fe^{3+}/\Sigma Fe$ ratios of minerals, indicating a linear relationship as a function of the $Fe^{3+}/\Sigma Fe$ ratio (e.g., Monkawa et al. 2006), and we can estimate the $Fe^{3+}/\Sigma Fe$ ratios of unknown samples with an accuracy of ±10 mol%. We employed two different kaersutite samples for Fe^{2+} and Fe^{3+} standards. The Fe^{2+} standard is kaersutite from Kaersut, Greenland which has a $Fe^{3+}/\Sigma Fe$ ratio of 0.01, and the Fe^{3+} standard is kaersutite from Iki, Japan which has a $Fe^{3+}/\Sigma Fe$ ratio of 0.93. The $Fe^{3+}/\Sigma Fe$ ratios of both standards were well characterised by wet chemistry (Monkawa et al., 2006).

The X-ray diffraction measurements were carried out using a micro-area diffraction equipment system installed in beam-line BL-4B1 at the Photon Factory, KEK (Ohsumi et al., 1995). A polychromatic X-ray microbeam was generated from synchrotron radiation by the micro pinhole put upstream of the sample.

The diameter of the microbeam is 1.6 µm on the sample position. A Laue photograph of the target sample was taken on a cylindrical imaging plate (Fuji Film Co. Ltd.) in an exposure time of 30 minutes.

3. Results

A back-scatter electron image of the Fe-oxide-bearing clast is shown in Figure 2. The clast has irregular boundaries, and is ~70 × 50 µm in size. It is composed of Fe-oxide (~47% by area, Table 1), enclosing disseminated troilite (62.8 wt% Fe, 36.2 wt% S; ~16% of area), and angular fragments of anorthite (An_{95-97}; Mg# 3-15; ~21% of area), pyroxene (En_{74-75},Fs_{21-22},Wo_{3-4}; Mg# 77; ~11% of area), and olivine (Fo_{66-67}; ~6% of area) (Table 2). The pyroxene and olivine fragments have Fe/Mn ratios that are typical of lunar lithologies (Fig. 3). These mafic minerals and the plagioclase fragments are compositionally similar to phases from ferroan to magnesian anorthosite lunar lithologies. The Fe-oxide is in a more massive form at the right hand edge of the clast. This region is surrounded by weak NE to E-W banding of Fe-oxide complimented by sub-micron sized pores and disseminated rounded troilite blebs. Outside of this banded area the Fe-oxide is intergrown with larger sub-angular troilite and angular plagioclase fragments and mafic minerals (Fig. 2a). The clast overall has a similar brecciated texture as fragments of sulphide-silicate mineral intergrowths in some 60016,83 impact melt breccias (Fig. 4).

The Fe-oxide has an average composition consistent with spinel-group magnetite (on the basis of 24 cations per 32 oxygens) (Table 1). Trace elements include CaO (0.17±0.10 wt%.), SiO_2 (0.15±0.06 wt%), Al_2O_3 (0.03±0.12 wt%) and MgO (0.01±0.05 wt%). Alkali element abundances are also low (Na is below detection limits of 0.06 wt% and K is below detection limits of 0.03 wt%). Transition metal Ti, Ni and Co contents in the magnetite are low (*e.g.*, below EMP detection limits of 0.04 wt%, 0.08 wt% and 0.06 wt% respectively).

We analysed three different spots of Fe-oxide by Fe micro-XANES in the more massive area of Fe-oxide. The obtained XANES spectra are all similar and clearly show that they are mixtures of both Fe^{2+} and Fe^{3+} (Fig. 5). The estimated $Fe^{3+}/\Sigma Fe$ ratio is ~0.45, which is close to the composition of magnetite.

A very complicated diffraction pattern was obtained (Fig. 6) from the XRD analysis suggesting that multiple domains exist in the irradiated area. A total of 700 diffraction spots (417 back and 283 transmission reflections) were collected in the pattern (Table 3). In order to assign indices, it was necessary to classify the attribution of diffraction spots to each domain. We found several sets of diffractions that belong to the same zone. When a diffraction spot exists on the intersection of zones, these diffractions were assumed to belong to the same domain. The indexing was made by comparison of interplanar angle obtained by the positions of diffractions, and the angle calculated by cell parameters. Indexing for hematite does not fit with the observed data. However, a total of 189 diffraction spots (120 back and 69 transmission reflections) were indexed by assuming the sample was magnetite. A new domain was found following the same procedure and the remaining diffraction spots were also indexed as magnetite. In total, we found four domains following the same approach and the results are summarised in Table 3. We ran a simulation of the diffraction patterns using the intensities and positions obtained from the magnetite structure, and they are good agreement with the observed diffraction images (Figs. 6a-d). Furthermore, when the calculated intensities are compared with two domains whose diffractions are comparatively strong, the weighted residual factors $R_w = [\Sigma w(I_{obs}-k\ I_{cal})^2 / \Sigma w\ I_{obs}^{\ 2}]^{1/2}$ are 0.079 and 0.119 respectively (where I_{obs} and I_{cal} are observed and calculated Laue intensities, k is a scale factor, and a w (unit weight) = 1). Therefore, it was confirmed that the four identified domains are all magnetite.

We could not index a further 138 diffractions (62 back and 76 transmission reflections) as their intensities were relatively weak and three or more reflections among them do not relate to the same zone. We interpret that these reflections were diffracted from many small domains, consistent with the textural observation of the complex clast (Fig. 2).

4. Discussion

4.1 Temporal Constraints for Formation

The magnetite is found in a clast within regolith breccia 60016. The 60016 sample is a B_2-type breccia characterised with a pale matrix and dark clasts (Wilshire et al., 1981) and is ancient regolith breccia

characterised by a high abundance of parentless 'trapped' ^{40}Ar (McKay et al., 1986; Joy et al. 2011). Previously no significant remnant magnetisation has been recorded within the breccia (Nagata et al., 1974, 1975; Cisowski et al., 1975), suggesting that magnetite is an uncommon component of sample 60016. The regolith breccia was collected from Apollo 16 Station 0 (close to the lunar lander), which is located on the Cayley Formation. This deposit was emplaced by ballistic sedimentation during the Imbrium basin-forming event (estimates of Imbrium basin age range from 3.85 Ga to 3.91 Ga: Stöffler et al., 2006 and references therein; Liu et al., 2012). The deposit is formed from distal Imbrium impact melt ejecta mixed with local pre-basin lunar crust and contributions of older basin ejecta (Nectaris, Serenitatis and others: Spudis, 1984; Stöffler et al., 1985; McKay et al., 1986; Korotev, 1996, 1997; Haskin et al., 2003; Petro and Pieters, 2006; Joy et al., 2011).

Joy et al. (2011) used the ratio of trapped ^{40}Ar to solar-wind derived ^{36}Ar to show that the components of 60016 were likely consolidated into a breccia (*e.g.,* closed from further regolith processing) at ~3.8 Ga, during the final stages of lunar basin-formation (Joy et al., 2012). Therefore, the magnetite-bearing fragment was likely incorporated into the 60016 parent regolith prior to ~3.8 Ga. This age constraint could imply (i) that the fragment was formed and included within the local Apollo 16 regolith during or after the emplacement of Cayley Formation at ~3.85 Ga, but before the breccia was consolidated at ~3.8 Ga; or (ii) that it was sourced from a pre-existing lithology in the local highlands crust or older basin ejecta at the Apollo 16 landing site (>3.85 Ga rocks), and then was included within the Cayley Formation during emplacement of the Imbrium ejecta sheet. In either case, the formation mechanism for the magnetite-bearing clast can be considered an 'ancient' >3.8 Ga lunar process.

4.2 Formation Mechanisms

The presence of magnetite in sample 60016 indicates that oxygen fugacity during formation were equilibrated at, or above, the wűstite-magnetite (WM) oxygen buffer (where fO_2 is temperature dependent) to buffer the valence change of Fe^{2+} to Fe^{3+}. This implies a more oxidised formation environment than is typically associated with either lunar surface or lunar interior conditions (Wadhwa, 2008 and references therein). However, the sample must have formed in conditions below the magnetite-hematite oxygen buffer as no hematite is observed in the 60016,83 assemblage.

Previous studies have suggested several processes for the production of ferric iron species (like magnetite) on the Moon. Exogenous sources include (1) direct delivery of Fe^{3+}-bearing mineral species in surviving meteorite fragments (as in the case of the magnetite-bearing Bench Crater meteorite), and (2) shock decomposition of hydrous minerals delivered to the lunar surface by hydrated impactors (*e.g.*, Wasilewski, 1973). Endogenic sources include (3) ferrous or metallic iron mineral oxidation or direct condensation from oxidising gases vented from fumaroles or degassing lava-flows (*e.g.*, Williams and Gibson, 1972; Shearer et al., 2014) and (4) direct crystallisation from an oxidised magmatic melt. Hybrid exogenous-endogenous formation model might include (5) direct mineral condensation (*e.g.*, Dikov et al., 2009; Yakovlev et al., 2009) or hydrothermal alteration of Fe-metal minerals by gases released during impact of a hydrous comet or carbonaceous-asteroid (*e.g.*, Williams and Gibson, 1972), or an anhydrous impactor projectile striking polar ices or a volatile-rich regolith (i.e., with an added solar wind or added meteoritic component: e.g., Liu et al., 2012; Stephant and Robert, 2014).

The 60016,83 magnetite-bearing clast is brecciated and includes poorly banded structures of magnetite intergrown with disseminated troilite, small (<1 µm) fragments of plagioclase and pore-spaces (Fig. 2a). The magnetite also encloses larger (>5 µm) angular to subangular clasts of lunar-derived silicate minerals (Fig. 2). This observation suggest that the fragment was formed *in situ* (*e.g.*, it is autochthonous) within the lunar regolith, rather than having been formed and transported to the lunar surface as an intact fragment of a magnetite-rich meteorite. Thus, formation mechanism (1) i.e., a surviving fragment of a magnetite-bearing projectile is unlikely. It is also unlikely that the magnetite originates from the shock decomposition of hydrous minerals (*e.g.*, biotite, amphibole, phyllosilicate) delivered by impactors (*i.e.*, mechanism (2)) as no glass component (Fig. 2) is preserved from a bi-product from breakdown of these minerals to magnetite (Wasilewski, 1973). Direct crystallisation from a lunar magmatic melt (*i.e.*, mechanism (4)) is unlikely as the clast is a breccia and does not have a crystalline igneous texture. Here, we consider the other plausible formation mechanisms. Magnetite can be formed by several pathways involving oxidation of Fe-metal or desulphurisation of FeS (troilite) in the presence of water or carbon dioxide across a range of partial pressures and temperatures. These pathways are illustrated in Figures 7 and 8 via the following net thermochemical reactions:

Metallic iron redox reactions (Figs. 7 and 8) are represented by the net reactions:

$$3Fe(s) + 4H_2O(g) = Fe_3O_4(s) + 4H_2(g) \quad (1)$$

$3Fe(s) + 4CO_2(g) = Fe_3O_4(s) + 4CO(g)$ (2)

Redox reactions involving wustite ($Fe_{1-x}O$) and magnetite (Figs. 7 and 8) are represented by:

$3FeO(s) + H_2O(g) = Fe_3O_4(s) + H_2(g)$ (3)

$3FeO(s) + CO_2(g) = Fe_3O_4(s) + CO(g)$ (4)

Desulphurisation/sulphurisation reactions between FeS and Fe_3O_4 (Fig. 8) are represented by the net reactions:

$3FeS(s) + 4H_2O(g) = Fe_3O_4(s) + 3H_2S(g) + H_2(g)$ (5)

$3FeS(s) + 4CO_2(g) = Fe_3O_4(s) + 3COS(g) + CO(g)$ (6)

where (s) indicates the solid phase and (g) indicates the gas phase.

As the oxidising species on the Moon is most likely OH (Sharp et al., 2013; Bell et al., 2015; McCubbin et al., *In Press*) the reaction:

$3Fe + 4OH = Fe_3O_4 + 2H_2$ (7)

may also be considered. In this case oxidation by OH will occur if the fugacity constraints given by the net reactions 1-6 are met, as OH equilibria is tied to the H_2O/H_2 ratio (e.g., $2OH + H_2 = 2H_2O$) and the oxygen fugacity of the system.

These oxidation- and desulphurisation-driven mineral replacements (*e.g.*, West, 1956; Hong and Fegley 1998; Fegley, 2000; Sakamoto et al., 2007; Plaul et al., 2009) are associated with a range of thermodynamic conditions, however, as there is no change in the number of gas molecules exchanged, these reactions are pressure independent (Fegley, 2000). In any of these thermochemical reactions, a

source of excess oxidising gas is desirable to drive the reactions to the right. Oxidising species present as a fluid will also facilitate oxidations via reactions 1, 3 and 5, with reduced gaseous by-products being degassed from the system. In this scenario, under equilibrium conditions, degassing of H_2 and CO will be compensated by simultaneous oxidation of the solid buffering phase (and simultaneous reduction of available CO_2 or H_2O) until exhaustion of the buffer (Nadeau et al., 2010; Sharp et al., 2013). Producing the relatively oxidising reactants (i.e., H_2O and CO_2 in equations 1 to 6) is a challenge on the Moon where reduced conditions dominate (Wetzel et al., 2013), and possible sources are explored in the next few sections.

4.2.1 Low temperature mineral alteration during solid-gas-liquid exchange: Magnetite can be converted from low-Ni-Fe-metal (e.g., in the representative reactions 1 and 2) at low temperatures (<570 °C) in equilibrium with H_2O steam or liquid, or CO_2 (Figs. 7 and 8) (Williams and Gibson, 1973; Hirano and Somiya, 1976; Plaul et al., 2009). At 300°C this conversion can occur at relatively low H_2O/H_2 (> 0.05) or CO_2/CO (> 1.9) (log $fO_2 \approx$ -41.9 ≈ IM), up to 570°C where H_2O/H_2 > 0.3 or CO_2/CO > 1.05 (log $fO_2 \approx$ -25.91 ≈ IM ≈ WM) will produce magnetite.

Conversion of Fe-metal to magnetite (Rubin, 1991; Hong and Fegley, 2010) has a positive volume change as Fe_3O_4 (44.52 cm^3 mol^{-1}) has a larger molar volume than Fe (7.1 cm^3 mol^{-1}) (Equations 1 and 2). As no Fe-metal is observed in the clast (Fig. 2), this could indicate complete conversation of Fe to Fe_3O_4. However, Fe-metal found on the Moon typically has a minor Ni-component (*i.e.*, it is kamacitic): in the case of indigenous lunar magmatic Fe-metal, Ni concentrations typically are <7 wt% Ni (Papike et al., 1991), where as in exogenously added meteoritic metal, Ni concentrations can be >3 wt% up to 20 wt% or more (*i.e.*, taenitic). Oxidation of kamacite metal (be it indigenous or meteoritic) would, therefore, result in the enrichment of Ni-metal alloys within the oxide construct or oxidation of Ni to form NiO-bearing magnetite (Hong and Fegley, 1998). We do not observe any Ni-bearing phases within the oxide assemblage: indicating that either the parent Fe-metal had very low Ni concentrations, or that Ni-bearing phases were removed from the system during the reaction, or that conversion of Fe-metal to magnetite (Equations 1 and 2) cannot account for the 60016,83 magnetite formation process.

4.2.2 High temperature mineral alteration during solid-gas-liquid exchange or high-temperature condensate: Oxidation of FeO species (Equations 3 and 4) associated with high temperature (>570 °C) equilibrium processes require higher oxygen fugacities (above IW buffer at 570°C, to +2.2 IW at 1000°C) with higher H_2O/H_2 or CO_2/CO partial pressures (Fig. 7), which are outside the range for known lunar surface and magmatic systems (Wadhwa, 2008 and references therein). If Fe was oxidised from FeO-bearing silicate minerals, we might expect to observe unusual Fe-mineral chemistry trends. However, this is not the case: for example, Fe/Mn ratios in olivine and pyroxene minerals (Table 2, Fig. 3) are compositionally similar to Apollo 16 feldspathic rocks. Thus, the FeO conversion to Fe_3O_4 scenario seems unlikely.

An alternative mechanism to potentially generate magnetite is through desulphurisation of troilite or pyrrhotite (Equations 5 and 6: Fig. 8), by an oxidising reactant. Pathways involving desulphurisation of pyrite (FeS_2) (Nadeau et al., 2010), or ferric-(hydro) oxides (Ohmoto, 2003) are not considered here as these phases are not observed in the 60016,83 magnetite-bearing clast and pyrite has not been reported in lunar samples. Likewise, desulphurisation of FeS by SO_2 gas is not considered, as elemental sulphur, a common by-product of this reaction, is not observed in the assemblage. Reactions weathering troilite to magnetite have a negative volume change as 3 molecules of FeS (18.2 cm^3 mol^{-1}) are required to convert to Fe_3O_4 (44.52 cm^3 mol^{-1}) (Equations 5 and 6). This is consistent with the low porosity of magnetite-bearing fragment (Fig. 2) and the presence of FeS phases throughout the fragment (Fig. 2). This desulphurisation process will be subject to the same constraints on fO_2, as indicated in Figure 8. For example, the conversion of FeS to Fe_3O_4 only occurs above either the IM or WM fugacity buffers

5. Potential Sources of Oxidising Species

Two oxidising agents - H_2O (liquid or steam) and CO_2 (Figures 7 and 8) - are considered here to be potentially responsible for creating the anomalously high lunar oxygen fugacity state conditions in which the 60016,83 magnetite assemblage was formed. Here, we consider the potential sources of these agents:

5.1 Endogenic source(s) of oxidising agents: There is also an ongoing paradigm shift that the Moon may be more hydrated and volatile rich than has been previously appreciated (see Anand et al., 2014, Robinson and Taylor, 2014; McCubbin et al., *In Press* for detailed reviews). For example, lunar basalt vesicles and vugs and the coatings of volcanic glass beads (pyroclastic glass) have shown deposits rich in volatile elements like S, Cl, Zn, Cu, Br, I and Fl derived from condensates from volatile-rich volcanic gases (Meyer, 1990; McKay and Wentworth, 1993). Picritic pyroclastic glass (Saal et al., 2008, 2013; Hauri et al., 2014) and melt inclusions within olivine hosted in orange picritic glass (Hauri et al., 2011) have shown that in some places the lunar mantle may be as hydrated as terrestrial mid-ocean ridge basalts (Hauri et al., 2011, 2014; McCubbin et al., *In Press*). Likewise, the ubiquitous presence of hydrated apatite in lunar rocks also provide evidence that different sources in the lunar mantle were water-bearing (Boyce et al., 2010; McCubbin et al., 2010; Greenwood et al., 2011; Tartèse et al., 2013, 2014; Barnes et al., 2014). Plausibly, if H_2O was a fluid in lunar magmatic systems (Bell et al., 2015), H_2O steam could be released during volcanic eruptions / fumaroles, providing a source for enhanced lunar oxidation conditions (Kring, 2014).

Lunar glass beads and basalts (Saal et al., 2008; Mortimer et al., *In Press*; McCubbin et al., *In Press* and references therein) have very low C-contents suggesting that reducing H_2 (over CO) was likely the main driver of volcanic eruptions (Hirschmann, et al., 2012; Sharp et al., 2013; Wetzel et al., 2014; Bell et al., 2015; McCubbin et al., *In Press*). Reaction of such magmatic H_2 with silicate and sulphide minerals has been invoked to explain secondary mineralisation and sulphide veining observed in lunar crustal rocks (Shearer et al., 2013; 2014; Sharp et al., 2013; Bell et al., 2015). However, CO and CH_4 and, to a lesser extent, CO_2 may have contributed to the rapid ascent of magma generating pyroclastic explosive events responsible for forming lunar picritic glass beads (Fegley, 1991) (C-rich gases are thought to be liberated when graphite or was oxidised in ascending magmas to shallow depths in the lunar crust: Sato et al., 1973; Sato, 1979; Fogel and Rutherford, 1995; Nicholis and Rutherford, 2009; Wetzel et al., 2014). If present, CO_2-species may, therefore, also have played a minor role in generating localised oxidation conditions during volcanic degassing episodes (Colson, 1991).

The composition of mafic mineral and plagioclase found in association with the 60016,83 magnetite-bearing clast, suggests that they are affiliated with lunar feldspathic (ferroan-magnesian anorthosite) lithologies, rather than mare basalt derived material. Therefore, if volcanic fumarolic gases were

responsible for the oxidising conditions that weathered the Fe-bearing mineral, then outgassing events took place within the feldspathic highlands as mare basalt lava-flows and eruption centres (i.e., pyroclastic vent sites) are located >280 km away from the Apollo 16 landing site. Krähenbühl et al. (1973) proposed that enrichment of volatile relative to involatile elements (*e.g.*, high Tl/Cs and Tl/U) in Apollo 16 regolith breccias, like 60016, could have been caused by an enhancement of (sporadic?) fumarolic activity in the lunar highlands >3.8 Ga prior to the main period of mare volcanism. Similar highlands magmatic degassing events may even still occur at the present day in heavily cratered area of lunar highlands where episodic earthquakes induce magmatic gas release along deep set fractures (Lawson et al., 2005).

5.2 Exogenous source(s) of oxidising agents: Surface volatile reservoirs may also be responsible for enhanced oxidising condition in or on the lunar regolith. Interpretation of 3-micron band spectral reflectance data has been interpreted to mean that OH and H_2O may temporarily be formed on the surface of regolith particles, as a result of solar wind liberation of O-atoms combining with implanted H-atoms (Clark, 2009; Pieters et al., 2009; Sunshine et al., 2009; see also Liu et al., 2012; Stephant and Robert, 2014). Remote sensing missions have also shown that at the present time, permanently shadowed regions of the lunar poles may have concentrated ice and other volatiles (Nozette et al., 1996, 2001; Feldman et al., 1998; Spudis et al., 2010; Neish et al., 2011). For example, the LRCOSS mission recently showed that hydrogen-bearing species are present in near-surface regoliths in Cabeus crater at concentrations of 5.6 ± 2.9 % (Colaprete et al., 2010). However, it is debatable as to whether these sort of volatile-rich reservoirs represent degassed primitive water and/or if it has been added over time by impacting comets and hydrated carbonaceous projectiles. Melting and vaporisation of such polar ice deposits by impacting projectiles may release H_2O liquid and steam to cause aqueous alteration and weathering of Fe-rich phases in an oxidised environment. However, it is unclear whether these polar ice reservoirs would have been stable prior to 2 Ga as the Moon had a higher obliquity causing polar illumination and limiting the conditions for ice preservation (Seigler et al., *In Press*). Regardless, 60016 was collected over a thousand km away from either pole, so in this case melted ice as a hydration/oxidation medium seems unlikely.

Alternatively, water and carbon-bearing species may have been delivered to other areas of the lunar regolith by impacting comets and carbonaceous chondritic projectiles throughout lunar history (*e.g.*, Gibson and Moore, 1973; Zolensky, 1996; Steele et al., 2010; Joy et al., 2012). Hydrogen, C and S gas

species, therefore, could be easily librated in impact plumes or, if they survive the impact process, would form potential reservoirs in the lunar regolith that could be mobilised as oxidising gas or fluid phases during subsequent impact events (McKay et al., 1972; Haskin and Warren, 1991). Volatile element enrichments measured in some Apollo 16 regoliths, for example, soil 61221 (Gibson and Moore, 1973; Hughes et al., 1973), and carbon-rich coatings on the surfaces of glasses (Thomas-Keprta et al., 2014), have been attributed to such exogenous implantation by a cometary or carbonaceous chondrite impactor. However, Shearer et al. (2014) argue that the majority of volatile elements and Cl-isotopic signatures in Apollo 16 rocks are not consistent with known groups of meteorites, and conclude that for the majority of these samples meteoritic material is not the main volatile source. It is possible though that projectile impacts and ejecta blanket emplacement provided high temperature surficial heating (1000-1200°C: McKay et al., 1972; Haskin and Warren, 1991) of the local lunar rocks and soils to liberate indigenous volatiles and cause thermal vapour transport of such species (Shearer et al., 2014). Such gases may have provided oxidising agents in the lunar regolith responsible for the types of reactions described here and facilitating secondary mineralisation and metal-silicate reactions observed in lunar rocks (Taylor et al., 1974; Hunter and Taylor, 1981; Shearer et al., 2013, 2014).

Conclusions

This study has identified an Fe-oxide bearing brecciated clast in lunar regolith breccia 60016 (Figs. 1 and 2). We have demonstrated using mineral compositions (Table 1), characteristic synchrotron XRD patterns (Table 2, Fig. 6) and XANES $Fe^{3+}/\Sigma Fe$ ratios (Fig. 5) that the Fe-oxide phase is magnetite. This is the first time that magnetite has been identified in a lunar sample using multiple analytical techniques. We have explored possible oxidation formation reactions with the most probably being desulphurisation from troilite to magnetite in the presence of CO_2 gas or H_2O steam or liquid at temperatures <570 °C (Fig. 8, Equations 5 and 6). The banding structure of some regions of the magnetite may suggest that this replacement and magnetite precipitation occurred in a mineralised vein or regolith pore spaces. The possible sources of oxidising agents range from low-temperature volcanic gases to impact vapour plume clouds to impact-driven degassing of volatile-bearing regoliths.

Although the magnetite fragment we have identified is only a few tens of microns in size, its discovery supports recent identification of other types of Fe-oxides (i.e., akaganéite) in Apollo 16 samples (Shearer et al., 2014) and theoretical models by Williams and Gibson (1972) that oxidised conditions may be a common low temperature state in the near surface environment of the Moon. Thus, it may be the case that Fe-oxides are present widely on the Moon in locations where periodic degassing or fluid release/migration occurs. Examples may include regoliths in lunar polar regions where ice/clathrates are present in partially or permanently shadowed craters (e.g., Spudis et al., 2010; Colaprete et al., 2010). In such environments H_2O and CO_2 may easily be liberated during heating episodes and become available to drive mineral replacement of Fe-metal or Fe-sulphide. Analysis of *in situ* mineralogical spacecraft instrument data (e.g., RAMAN, XRD, Mössbauer) and study of returned samples from future missions to polar localities could test this hypothesis.

Acknowledgements

Thanks to Anne Peslier and Kent Ross for laboratory assistance at JSC. Thanks to CAPTEM for Apollo sample allocation. Thanks to Romain Tartèse for helpful discussions. We thank the helpful reviews by Malcolm Rutherford and an anonymous reviewer and the editorial guidance of Randy Korotev to help improve this manuscript. This research was funded by NASA Lunar Science Institute cooperative NNA09DB33A and Solar System Exploration Research Virtual Institute cooperative agreement NNA14AB07A (David A. Kring PI). KHJ also acknowledges Leverhulme Grant 2011-569. SR-XRD and SR-XANES analyses were performed by the Photon Factory research programs #2010G142 and #2010G534, respectively. This is LPI contribution number 1837.

References

Anand M., Tartèse R., and Barnes J. J. 2014. Understanding the origin and evolution of water in the Moon through lunar sample studies. *Philosophical Transactions of the Royal Society A* 372:20130254. doi: 10.1098/rsta.2013.0254

Agrell S. O., Scoon J. H., Long J. V. P., and Coles J. N. 1972. The Occurrence of Geothite in a Microbreccia from the Fra Mauro Formation (abstract). 3rd Lunar Science Conference. pp. 7–9.

Barnes J. J., Tartèse R., Anand M., McCubbin F. M., Franchi I. A., Starkey N. A., and Russell S. S. 2014. The origin of water in the primitive Moon as revealed by the lunar highlands samples. *Earth and Planetary Science Letters* 390:244–252. doi:10.1016/j.epsl.2014.01.015.

Bell A. S., Shearer C., J. de Moor M., and Provencio P. 2015. Using the sulfide replacement textures in lunar breccia 67915 to construct a thermodynamic model of H-S-O-C fluids in the lunar crust (abstract #2479). 46th Lunar and Planetary Science Conference.

Boyce J. W., Liu Y., Rossman G. R., Guan Y., Eiler J. M., Stolper E. M., and Taylor L. A. 2010. Lunar apatite with terrestrial volatile abundances. *Nature* 466:466–469.

Colaprete A., Schultz P., Heldmann J., Wooden D., Shirley M., Ennico K., Hermalyn B., Marshall W., Ricco A., Elphic R. C., Goldstein D., Summy D., Bart G. D., Asphaug E., Korycansky D., Landis D., and Sollitt L. 2010. Detection of water in the LROSS ejecta plume. *Science* 330:463–468. doi: 10.1126/science.1186986.

Cisowski S.M., Fuller M. D., Wu Y.-M., Rose M. F., and Wasilewski P. J. 1975 Magnetic effects of shock and their implications for magnetism of lunar samples. Proceedings, 6th Lunar Science Conference. pp. 3123–3141.

Chase M.W. 1998. NIST-JANAF thermochemical tables. *J. Phys. Chem. Ref. Data* 28, Monograph No. 9. 1951 pp.

Clark R. N. 2009. Detection of Adsorbed Water and Hydroxyl on the Moon. *Science* 326:562–564.

Colson R. O. 1991. Mineralization on the moon? Theoretical considerations of Apollo 16 'rusty rocks', sulfide replacement in 67016, and surface-correlated volatiles on lunar volcanic glass. Proceedings, 22nd Lunar and Planetary Science. pp. 427–436.

Crawford I. A., Fagents S. A., Joy K. H., and Rumpf M. E. 2010. Lunar Palaeoregolith Deposits as Recorders of the Galactic Environment of the Solar System and Implications for Astrobiology. *Earth, Moon and Planets* 107:75-85. doi:10.1007/s11038-010-9358-z

Dikov Yu. P., Gerasimov M. V., Yakovlev O. I., and A. V. Ivanov. 2009. Valence State of Iron in a Condensate from the Luna 16 Regolith. *Petrology* 17:429–438.

Drake M. J. 1975. The oxidation state of europium as an indicator of oxygen fugacity *Geochimica et Cosmochimica Acta* 39:55–64.

Dabrowski A., Mendyk E., Robens E., Skrzypiec K., Goworek J., Iwan M., and Rzaczyaska Z. 2008. Investigation of surface properties of lunar regolith Part III. *Journal of Thermal Analysis and Calorimetry* 94:633–639

Fagan A. L., Joy K. H., Bogard D. D., and Kring D. A. 2014. Ages of globally distributed lunar paleoregoliths and soils from 3.9 Ga to the present day. *Earth, Moon and Planets* 112:59–71. doi: 10.1007/s11038-014-9437-7.

Fegley B. Jr. 2000. Kinetics of gas-grain reactions in the solar nebula. *Space Science Reviews* 92:177–200.

Fegley B. Jr. 2013. Practical Chemical Thermodynamics for Geoscientists. Waltham, M A: Academic Press . 674 pp.

Feldman W. C., Maurice S., Binder A. B., Barraclough B. L., Elphic R. C., and Lawrence D. J. 1998. Fluxes of Fast and Epithermal Neutrons from Lunar Prospector: Evidence for Water Ice at the Lunar Poles. *Science* 281:1496–1500. doi: 10.1126/science.281.5382.1496.

Fogel R. A., and Rutherford M. J. 1995 Magmatic volatiles in primitive lunar glasses: I. FTIR and EPMA analyses of Apollo 15 green and yellow glasses and revision of the volatile-assisted fire-fountain theory. *Geochimica et Cosmochimica Acta* 59: 201–215

Forester D. W. 1973. Mössbauer search for ferric oxide phases in lunar materials and simulated lunar materials. Proceedings, 4th Lunar Science Conference. pp. 2697–2707

Fun-Dow T., Manatt S. L., and Chan S. I. 1973. Magnetic phases in lunar fines: metallic Fe or ferric oxides? *Geochimica et Cosmochimica Acta* 37:1201–1211. doi:10.1016/0016-7037(73)90056-2.

Gibson E. K. Jr., and Moore G. W. 1973. Volatile-Rich Lunar Soil: Evidence of Possible Cometary Impact Source. *Science* 179:69–71.

Greenwood J. P., Itoh S., Sakamoto N., Warren P., Taylor L., and Yurimoto H. 2011. Hydrogen isotope ratios in lunar rocks indicate delivery of cometary water to the Moon. *Nature Geoscience* 4:79–82. doi:10.1038/ngeo1050

Griscom D. L., and Marquardt C. L. 1972. Evidence of lunar surface oxidation processes: electron spin resonance spectra of lunar materials and simulated lunar materials. Proceedings, 3rd Lunar Science Conference. pp. 2397–2415.

Griscom D. L. 1974 Ferromagnetic resonance spectra of lunar fines: some implications of line shape analysis. *Geochimica et Cosmochimica Acta* 38:1509–1519. doi:10.1016/0016-7037(74)90171-9.

Gurvich L. V., Veyts I. V., and Alcock C. B. 1989. Thermodynamic Properties of Individual Substances, fourth ed., vol. 1, parts 1 and 2. New York: Hemisphere Publishing. 929pp.

Haggerty S. E. 1978. Apollo 16 Deep Drill: Morphological Characteristics of Oxyhydrates on Rusty Particle 60002,108. Proceedings, 9th Lunar and Planetary Science Conference. pp. 442–444.

Hauri E. H, Weinreich T., Saal A. E., Rutherford M. C., and Van Orman J. A. 2011. High Pre-Eruptive Water Contents Preserved in Lunar Melt Inclusions. *Science* 333:213–215.

Hauri E. H., Saal A. E. , Rutherford M. J., and Van Orman J. A. 2015. Water in the Moon's interior: Truth and consequences. *Earth and Planetary Science Letters* 409:252–264.

Haskin L. A., and Warren P. 1991 Lunar Chemistry. In Lunar Source Book (eds. G. H. Heiken, D. T. Vaniman and B. V. French). Cambridge University Press, Cambridge, pp. 357–474.

Haskin L. A., Moss B. E., and McKinnon W. B. 2003. On estimating contributions of basin ejecta to regolith deposits at lunar sites. *Meteoritics and Planetary Science* 38:13–33.

Hirano S., and Somiya S. 1976. Hydrothermal crystal growth of magnetite in the presence of hydrogen. *Journal of Crystal Growth* 35:273–278.

Hirschmann M.M., Withers,A.C., Ardia P., and Foley N.T. 2012. Solubility of molecular hydrogen in silicate melts and consequences for volatile evolution of terrestrial planets. *Earth and Planetary Science Letters* 345:38–48.

Hong Y., and Fegley B. Jr. 1998. Experimental Studies of Magnetite Formation in the Solar Nebula, *Meteoritics and Planetary Science* 33:1101–1112.

Hörz F., Grieve R., Heiken G., Spudis P., and Binder A. 1991 Lunar surface processes. In *Lunar Sourcebook*, edited by Heiken G., Vaniman D., and French B.M. Cambridge: Cambridge University Press. pp. 1-120.

Housley R. M., Cirlin E. H., Paton N. E., and Goldberg I. B. 1974. Solar wind and micrometeorite alteration of the lunar regolith. Proceedings, 5th Lunar Science Conference. pp. 2323–2642.

Hughes T. C., Keays R. R. and Lovering J. F. 1973. Siderophile and volatile trace elements in Apollo 14, 15 and 16 rocks and fines: evidence for extra lunar component and Tl-, Au- and Ag enriched rocks in the ancient lunar crust (abstract). 4th Lunar Science Conference. pp. 400–402.

Hunter R. H., and Taylor L. A. 1981. Rust and schreibersite in Apollo 16 highland rocks - Manifestations of volatile-element mobility. Proceedings, 12th Lunar and Planetary Science Conference. pp. 253–259.

Jedwab J., Herbosch A., Wollast R., Naessens G., and van Geen-Peers N. 1970. Search for magnetite in lunar rocks and fines. *Science* 167:618–619.

Joy K. H., Kring D. A., Bogard D. D., McKay D. S., and Zolensky M. E. 2011. Re-examination of the formation ages of Apollo 16 regolith breccias. *Geochimica et Cosmochimica Acta*. 75:7208–7225. doi:10.1016/j.gca.2011.09.018.

Joy K. H., Zolensky M. E., Nagashima K., Huss G. R., McKay D. S., Ross D. K., and Kring D. A. 2012 Direct detection of projectile relics from the end of the lunar basin-forming epoch. *Science.* 336:1426-1429. doi 10.1126/science.1219633.

Joy K. H., Crawford I. A., Huss G., Nagashima K., and Taylor G. J. 2014. An unusual clast in lunar meteorite MacAlpine Hills 88105: a unique lunar sample or projectile debris? *Meteorites and Planetary Science.* 49:677–695. doi: 10.1111/maps.12270.

Karner J. M., Papike J. J., and Shearer C. K. 2004. Plagioclase from planetary basalts: Chemical signatures that reflect planetary volatile budgets, oxygen fugacity, and styles of igneous differentiation *American Mineralogist.* 89:1101–1109.

Karner J. M., Sutton S.R., Papike J. J., Shearer C.K., Jones J. H., and Newville M. 2006. Application of a new vanadium valence oxybarometer to basaltic glasses from the Earth, Moon, and Mars. *American Mineralogist* 91:270–277.

Kolopus J. L., Kline D., Chatelain A., and Weeks R. A. 1971. Magnetic resonance properties of lunar samples: mostly Apollo 12. Proceedings, 2nd Lunar Science Conference. pp. 2501–2514.

Korotev R. L. 1996. On the relationship between the Apollo 16 ancient regolith breccias and feldspathic fragmental breccias, and the composition of the prebasin crust in the Central Highlands of the Moon. *Meteorites and Planetary Science.* 31:403–412.

Korotev R. L. 1997. Some things we can infer from the Moon from the composition of the Apollo 16 regolith. *Meteorites and Planetary Science.* 32:447–478.

Krähenbühl U., Ganapathy R., Morgan J. W., and Anders E. 1973. Volatile elements in Apollo 16 samples: Implications for highland volcanism and accretion history of the moon. Proceedings, 4th Lunar Science Conference. p.1325-1348.

Kring D. A. 2014. Production of volatiles at lunar pyroclastic volcanic vents. Annual Meeting of the Lunar Exploration Analysis Group (abstract #3056).

Lawson S. L., Feldman W. C., Lawrence D. J., Moore K. R., Elphic R. C., and Belian R. D. 2005. Recent outgassing from the lunar surface: The Lunar Prospector Alpha Particle Spectrometer. *Journal of Geophysical Research* 110:E09009. doi:10.1029/2005JE002433.

Ling Z. C., Wang A., and Jolliff B. L. 2011. Mineralogy and geochemistry of four lunar soils by laser-Raman study. *Icarus* 211:101–113. doi:10.1016/j.icarus.2010.08.020.

Liu D., Jolliff B. L., Zeigler R. A., Korotev R. L., Wan Y., Xie H., Zhang Y., Dong C. and Wang W. 2012. Comparative zircon U-Pb geochronology of impact melt breccias from Apollo 12 and lunar meteorite SaU 169, and the age of the Imbrium impact. *Earth and Planetary Science Letters* 319–320:277–286.

Liu Y., Guan Y., Zhang Y., Rossman G. R., Eiler J. M. and Taylor L. A. 2 012. Direct measurement of hydroxyl in the lunar regolith and the origin of lunar surface water. *Nature Geoscience* 5:779–782. doi: 10.1038/NGEO1601

Longhi J. 1992. Experimental petrology and petrogenesis of mare volcanic. *Geochimica et Cosmochimica Acta.* 56:2235–2251.

Lucey P., Korotev R.L., Gillis J.J., Taylor L.A., Lawrence D., Campbell B.A., Elphic R., Feldmann B., Hood L.L., Hunten D., Mendillo M., Noble S., Papike J J., Reedy R.C., Lawson S., Prettyman T., Gasault O., and Maurice S. 2006. Understanding the lunar surface and Space-Moon interactions. In *New Views of the Moon*, eds. B. L. Jolliff, M. A. Wieczorek, C. K. Shearer, and C. R. Neal, *Rev. Mineral. Geochem*. 60:83–219.

McCubbin F. M., A.Steele, Haurib E. H., Nekvasil H., Yamashit S., and Hemley R. J. 2010. Nominally hydrous magmatism on the Moon. *Proceedings of the National Academy of Sciences* 107:11223–11228.

McCubbin F. M., Vander Kaaden K. E., Tartèse R., Klima R. L., Liu Y., Mortimer J., Barnes J. J., Shearer C. K., Treiman A. H., Lawrence D. J., Elardo S. M., Hurley D. M., Boyce J. W., and Mahesh Anand. *In Press.* Magmatic volatiles (H, C, N, F, S, Cl) in the lunar mantle, crust, and regolith: Abundances, distributions, processes, and reservoirs. *American Mineralogist.* DOI: 10.2138/am-2015-4934.

McKay D. S. and Wentworth S. J. 1993. Grain surface features of Apollo 17 orange and black glass (abstract). 24th Lunar and Planetary Science. pp. 961–962.

McKay D. S., Clanton U. S., Morrison D. A., and Ladle G. H. 1972. Vapor phase crystallization in Apollo 14 breccia. Proceedings, 3rd Lunar Science Conference. pp. 739–752.

McKay D. S., Bogard D. D, Morris R. V., Korotev R. L., Johnson P., and Wentworth S. J. (1986) Apollo 16 regolith breccias: Characterization and evidence for early formation in the mega-regolith. Proceedings, 16th Lunar and Planetary Science Conference. In *Journal Geophysical Research* 91: D277–D303.

McKay D. S., Bogard D. D, Morris R. V., Korotev R. L., Wentworth S. J., and Johnson P. 1989. Apollo 15 regolith breccias - Window to a KREEP regolith. Proceedings, 19th Lunar and Planetary Science Conference. pp. 19-41.

McKay D. S., Heiken G., Basu A., Blanford G., Simon S., Reedy R., French B. M., and Papike J. 1991. The Lunar Regolith. In *Lunar Sourcebook*, edited by Heiken G., Vaniman D., and French B. M. Cambridge: Cambridge University Press. pp. 286-356.

McSween H. Y. Jr. 1976. A new type of chondritic meteorite found in lunar soil. *Earth and Planetary Science Letters.* 31:193–199.

Meyer C. A. 1989. Brief Literature Review of Observations Pertaining to Condensed Volatile Coatings on Lunar Volcanic Glasses. Workshop on Lunar Volcanic Glasses: Scientific and Resource Potential. LPI Technical Report 90-02, p.50.

Monkawa A., Mikouchi T., Koizumi E., Sugiyama K. and Miyamoto M. 2006. Determination of the Fe oxidation state of the Chassigny kaersutite: A microXANES spectroscopic study. *Meteoritics and Planetary Science* 41:1321–1329. doi: 10.1111/j.1945-5100.2006.tb00524.x.

Mortimer J., Verchovsky A. B., Anand M., Gilmour I., and Pillinger C. T. *In Press*. Simultaneous analysis of abundance and isotopic composition of nitrogen, carbon, and noble gases in lunar basalts: Insights into interior and surface processes on the Moon. *Icarus*. doi:10.1016/j.icarus.2014.10.006

Nadeau O., Williams-Jones A. E., and Stix J. 2010. Sulphide magma as a source of metals in arc-related magmatic hydrothermal ore fluids. *Nature Geoscience* 3:501–505.

Nagata T., Sugiura N., Fisher R. M., Schwerer F. C., Fuller M. D., and Dunn J.R. 1974 Magnetic properties of Apollo 11-17 lunar materials with special reference to effects of meteorite impact. Proceedings, 5th Lunar Science Conference. pp. 2827–2839.

Nagata T., Fisher R. M., Schwerer F. C., Fuller M. D, and Dunn J. R. 1975. Effects of meteorite impact on magnetic properties of Apollo lunar materials. Proceedings, 6th Lunar Science Conference. pp. 3111–3122.

Neish C. D., Bussey D. B. J., Spudis P., Marshall W., Thomson B. J., Patterson G. W., and Carter L. M. 2011. The nature of lunar volatiles as revealed by Mini-RF observations of the LCROSS impact site. *Journal of Geophysical Research* 116:E01005, doi:10.1029/2010JE003647

Nicholis M. G., and Rutherford M. J. 2009. Graphite oxidation in the Apollo 17 orange glass magma: Implications for the generation of a lunar volcanic gas phase. *Geochimica et Cosmochimica Acta* 73: 5905–5917. doi:10.1016/j.gca.2009.06.022.

Nozette S., Lichtenberg C. L., Spudis P., Bonner R., Ort W., Malaret E., Robinson M., and Shoemaker E. M. 1996. The Clementine Bistatic Radar Experiment. *Science* 274:1495–1498. doi:10.1126 science.274.5292.1495.

Nozette S., Spudis P., Robinson M., Lichtenberg C. L., Bussey D. B. J., and Bonner R. 2001. Integration of lunar polar remote-sensing data sets: Evidence for ice at the lunar South Pole. *Journal Of Geophysical Research* 106:23253–23266.

Ohmoto H. 2003. Nonredox transformations of magnetite-hematite in hydrothermal systems. *Economic Geology* 98:157–161.

Ohsumi K., Hagiya K., Uchida M., Suda N., Miyamoto M., Kitamura M. and Ohmasa M. 1995. Development of a microarea diffraction system by polychromatic synchrotron radiation with the Laue method. *Review of Scientific Instruments* 66:1448–1450.

Papike J. J., Taylor L. A., and Simon S. 1991. Lunar Minerals. In *Lunar sourcebook: A user's guide to the moon*: Edited by Grant H. Heiken David Vaniman and Bevan M. French. Cambridge University Press, 1991. (ISBN 0-521-33444-6).

Papike J. J., Karner J. M., and Shearer C. K. 2005. Comparative planetary mineralogy: Valence state partitioning of Cr, Fe, Ti, and V among crystallographic sites in olivine, pyroxene, and spinel from planetary basalts. *American Mineralogist* 90:277–290. doi:10.2138/am.2005.1779.

Pasieczna-Patkowska S., Dabrowski A., Robens E., and Ryczkowski J. 2008. FT-IR/PAS Studies of Lunar Regolith Samples. *Acta Physica Polonica A. Optical and Acoustical Methods in Science and Technology* 114:A-163–168

Petro N. E. and Pieters C. M. 2006. Modeling the provenance of the Apollo 16 regolith. *Journal of Geophysical Research* 111, E09005. doi:10.1029/2005JE002559.

Pieters C. M., Goswami J. N., Clark R. N., Annadurai M., Boardman J., Buratti B., Combe J.-P., Dyar M. D., Green R., Head J. W., Hibbitts C., Hicks M., Isaacson P., Klima R., Kramer G., Kumar S., Livo E., Lundeen S., Malaret E., McCord T., Mustard J., Nettles J., Petro N., Runyon C., Staid M., Sunshine J., Taylor L. A., Tompkins S., and Varanasi P. 2009. Character and spatial distribution of OH/H_2O on the surface of the Moon seen by M3 on Chandrayaan-1. *Science* 326**:**568–572.

Plaul F. J., Böhm C., and Schenk J. L. 2009. Fluidized-bed technology for the production of iron products for steelmaking. *The Journal of The Southern African Institute of Mining and Metallurgy* 108:121–128.

Ramdohr P., and El Goresey A. 1970. Opaque Minerals of the Lunar Rocks and Dust from Mare Tranquillitatis Source. *Science* 167:615–618.

Robie R. A., and Hemingway B. S. 1995, Thermodynamic Properties of Minerals and Related Substances at 298.15 K and 1 Bar (105 Pascals) Pressure and at Higher Temperatures. Washington, DC: USGS Bulletin 2131). 461 pp.

Robinson K. L. and Taylor G. J. 2014. Heterogeneous distribution of water in the Moon. *Nature Geoscience* 7:401–408. doi:10.1038/NGEO2173.

Rubin A. E. 1991. Euhedral awaruite in the Allende meteorite: Implications for the origin of awaruite and magnetite-bearing nodules in CV3 chondrules. *American Mineralogist* 76:1356–1362.

Runcorn S. K., Collinson W., O'Reill Y W., Stephenson A., Battey M. H., Manson A. J., and Readman P. W. 1971. Magnetic properties of Apollo 12 lunar samples. *Proceedings of the Royal Society* 3258:157–174.

Saal A. E., Hauri E. H., Lo Cascio M., Van Orman J. A., Rutherford M.C., and Cooper R. F. 2008 Volatile content of lunar volcanic glasses and the presence of water in the Moon's interior. *Nature* 454:192–195. doi:10.1038/nature07047.

Saal A. E., Hauri E. H., Van Orman J. A., and Rutherford M. J. 2013. Hydrogen isotopes in lunar volcanic glasses and melt inclusions reveal a carbonaceous chondrite heritage. *Science* 340:1317–1320.

Sakamoto N., Seto Y., Itoh S., Kuramoto K., Fujino K., Nagashima K., Krot A. N., and Yurimoto H. 2007. Remnants of the early Solar System water enriched in heavy oxygen isotopes. *Science* 317:231–233

Sato M. 1979. The driving mechanism of lunar pyroclastic eruptions inferred from the oxygen fugacity behavior of Apollo 17 orange glass. Proceedings, 10th Lunar and Planetary Science Conference. pp. 311–325.

Sato M., Hickling N. L., and McLane J. E. 1973. Oxygen fugacity values of Apollo 12, 14, and 15 lunar samples and reduced state of lunar magmas. Proceedings, 4th Lunar Science Conference. pp.1061–1079.

Sharp Z.D., McCubbin F.M., and Shearer C.K. 2013. A hydrogen-based oxidation mechanism relevant to planetary formation. *Earth and Planetary Science Letters* 380:88–97.

Siegler M., Paige D., Williams J.-P., Bills B. (In Press) Evolution of lunar polar ice stability. *Icarus* doi:10.1016/j.icarus.2014.09.037

Shearer C. K., Papike J. J., and Karner J. M. 2006. Pyroxene europium valence oxybarometer: Effects of pyroxene composition, melt composition, and crystallization kinetics. *American Mineralogist* 91:1565–1573.

Shearer C. K., Burger P. V., Guan Y., Papike J. J., Sutton S. R. , Atudorei N. V. 2012. Origin of sulfide replacement textures in lunar breccias. Implications for vapor element transport in the lunar crust. *Geochimica et Cosmochimica Acta* 83:138–158.

Shearer C. K., Sharp Z. D., Burger P. V., McCubbin F. M., Provencio P. P., Brearley A. J., and Steele A. 2014. Chlorine distribution and its isotopic composition in“rusty rock” 66095. Implications for volatile element enrichments of “rusty rock” and lunar soils, origin of “rusty” alteration, and volatile element behavior on the Moon. *Geochimica et Cosmochimica Acta* 139:411–433. doi:10.1016/j.gca.2014.04.029.

Simon S. B., Papike J. J., Laul J. C., Hughes S. S., and. Schmitt R. A. 1988. Apollo 16 regolith breccias and soils: recorders of exotic component addition to the Descartes region of the moon. *Earth and Planetary Science Letters* 89:147–162.

Spudis P. D. 1984. Apollo 16 site geology and impact melts - Implications for the geologic history of the lunar highlands. Proceedings, 15th Lunar and Planetary Science Conference. In *Journal of Geophysical Research* 89:C95–C107.

Spudis P. D., and Taylor G. J. 2009. A Major KREEP-Basalt -Mare Basalt Unconformity on the Moon (abstract #1039). 40th Lunar and Planetary Science Conference.

Spudis P. D., Bussey D. B. J., Baloga S. M., Butler B. J., Carl D., Carter L. M., Chakraborty M., Elphic R. C., Gillis-Davis J. J., Goswami J. N., Heggy E., Hillyard M., Jensen R., Kirk R. L., LaVallee D., McKerracher P., Neish C. D., Nozette S., Nylund S., Palsetia M., Patterson W., Robinson M. S., Raney R. K., Schulze R. C., Sequeira H., Skura J., Thompson T. W., Thomson B. J., Ustinov E. A., and Winters H. L. 2010. Initial results for the north pole of the Moon from Mini-SAR, Chandrayaan-1 mission. *Geophysical Research Letters* 37:L06204. doi:10.1029/2009GL042259

Sunshine J. M., Farnham T. L., Feaga L. M., Groussin O., Merlin F., Milliken R .E., and A'Hearn M. F. 2009. Temporal and Spatial Variability of Lunar Hydration As Observed by the Deep Impact Spacecraft. *Science* 326:565–568.

Sutton S. R., Jones K.W., Gordon B., Rivers M. L., Bajt S., Smith J. V. 1993. Reduced chromium in olivine grains from lunar basalt 15555: X-ray Absorption Near Edge Structure (XANES) *Geochimica et Cosmochimica Acta* 57:461–46.

Steele A., McCubbin F. M., Fries M., Glamoclija M., Kater L., and Nekvasil H. 2010: Graphite in an Apollo 17 Impact Melt Breccia. *Science* 329:51. doi: 10.1126/science.1190541.

Stephant A. and Robert F. 2014. The negligible chondritic contribution in the lunar soils water *Proceedings of the National Academy of Sciences* 111:15007–15012. doi: 10.1073/pnas.1408118111.

Stöffler D., Bischoff A., Borchardt R.., Burghele A., Deutsch A., Jessberger E. K., Ostertag R., Palme H., Spettel B., Reimold W. U., Wacker K., and Wanke H. 1985. Composition and evolution of the lunar crust in the Descartes highlands, Apollo 16. Proceedings, 15th Lunar and Planetary Science Conference. In. *J. of Geophys. Res.* 90:C449-C506.

Stöffler D., Ryder G., Ivanov B.A., Artemieva N.A. Cintala M.J., and Grieve R.A.F. 2006. Cratering history and lunar chronology. In *New Views of the Moon*, eds. B. L. Jolliff, M. A. Wieczorek, C. K. Shearer, and C. R. Neal. *Rev. Mineral. Geochem.* 60:519–596.

Tartèse R., Anand M., Barnes J. J., Starkey N. A., Franchi I. A., and Sano Y. 2013. The abundance, distribution, and isotopic composition of Hydrogen in the Moon as revealed by basaltic lunar samples: Implications for the volatile inventory of the Moon. *Geochimica et Cosmochimica Acta* 122:58–74. doi:10.1016/j.gca.2013.08.014.

Tartèse R., Anand M., McCubbin F. M., Elardo S. M., Shearer C. K., and Franchi I. A. 2014. Apatites in lunar KREEP basalts: The missing link to understanding the H isotope systematics of the Moon. *Geology* 42:363–366.

Taylor L. A., and Burton, J. C. 1976. Experiments on the stability of FeOOH on the surface of the moon. *Meteoritics* 11: 225–230.

Taylor L. A., Mao H. K., and Bell P. M. 1974. Beta-FeOOH, akaganeite, in lunar rocks Proceedings, 5th Lunar Science Conference. pp. 743–748.

Thomas-Keprta K. L., Clemett S. J., Messenger S., Ross D. K., Le L., Rahman Z., McKay D. S., Gibson Jr. E. K., Gonzalez C., Peabody W. 2014. Organic matter on the Earth's Moon *Geochimica et Cosmochimica Acta* 134:1–15. doi:10.1016/j.gca.2014.02.047.

Wadhwa M. 2008. Redox Conditions on Small Bodies, the Moon and Mars. *Reviews in Mineralogy & Geochemistry* 68:493–510. doi:10.2138/rmg.2008.68.17.

Wasilewski P. J. 1973. Shock remagnetization associated with meteorite impact at planetary surfaces. *The Moon* 6:264–291.

Weeks R. A. 1972. Magnetic phases in lunar material and their electron magnetic resonance spectra. Proceedings, 3rd Lunar Science Conference pp. 2503–2517.

Weeks R. A., Kolopus J. L., Kline D., and Chatelain A. 1970. Apollo 11 lunar material: nuclear magnetic resonance of 27Al and electron resonance of Fe and Mn. Proceedings, 11th Lunar and Planetary Science Conference. pp. 2467–2490.

Weeks R. A., Kolopus J. L. and Kline D. 1972. Magnetic phases in lunar material and their electron magnetic resonance spectra: Apollo 14 (abstract). Lunar Science-III (editor C. Watkins), pp. 791-793. Lunar Science Institute Contrib. No. 88.

West J. R. 1956. Roasting pyrites. US Patent number 2772153.

Wetzel D. T.,, Rutherford M. J., Jacobsen S. D., Hauri E. H., and Saal A. E. 2013. Degassing of reduced carbon from planetary basalts. *Proceedings National Academy Sciences* 110:8010–8013

Wetzel D. T., Hauri E. H., Saal A. E., and Rutherford M. J. 2014. Dissolved carbon content of the lunar volcanic glass beads and melt inclusions: Carbon from the lunar interior. (abstract #2238). 45th Lunar and Planetary Science Conference.

Williams R. J., and Gibson E. K. 1972. The origin and stability of lunar goethite, hematite and magnetite. *Earth and Planetary Science Letters* 17:84–88.

Wilshire H. G., Stuart-Alexander D. E., and Schwarzman E. C. 1981. E. Petrology and distribution of returned samples. In Geology of the Apollo 16 Area, Central Lunar Highlands. *US Geological Survey Professional Paper 1048.* Edited by George E. Ulrich, Carroll Ann Hodges and William R. Muehlberger. US Government Printing Office, Washington, 1981.

Wilke M., Farges F., Petit P.-E., Brown G. E. Jr., and Martin F. 2001. Oxidation state and coordination of Fe in minerals: an Fe *K*-XANES spectroscopic study. *American Mineralogist* 86:714–730.

Yakovlev O. I., Dikov Yu. P., and Gerasimov M. V. 2009. Effect of the Disproportionation Reaction of Ferrous Iron in Impact–Evaporation Processes *Geochemistry International* 47: 134–142.

Zolensky M. E. 1997. Structural water in the Bench Crater chondrite returned from the Moon. *Meteoritics and Planetary Science* 32:15–18.

Zolensky M. E., Weisberg M. K., Buchanan P. C., and Mittlefehldt D. W. 1996. Mineralogy of carbonaceous chondrite calsts in howardites, eucrites and the Moon. *Meteoritics and Planetary Science.* 31:518–537.

Figure Captions

Figure 1. Left: Optical light image of thin section 60016,83. Middle: montaged back-scatter electron image of 60016,83. Indicated with the red arrow and box is the location of the magnetite-bearing fragment. Right: Montaged false-colour element map where colours denote qualitative distribution and abundance of Si (blue), Al (white), Mg (green), Fe (red), Ca (yellow) and Ti (pink). (n.b., horizontal black line in the BSE image and element map represents an area of the sample that was not mapped).

Figure 2. (a) Close-up back-scattered electron (BSE) image and (b) close-up reflected light image of the Fe-oxide bearing fragment in 60016,83. Dark grey phases are plagioclase, which dominates the mineralogy of the surrounding matrix. Black regions are cracks and pores. Light grey phase is magnetite. Lightest grey (BSE) / pastel-orange (reflected light) phases are FeS. (c) Minerals phases identified in the fragment (see Table 2 for composition). Black areas represent pores, fractures or phases that cannot be identified.

Figure 3. Fe (afu) vs. Mn (afu) in olivine (left) and pyroxene (right) in the 60016,83 magnetite-bearing clast. Data are compared with trends of samples from Mars, Vesta, chondrites and terrestrial rocks (fitted trends from Papike et al., 2009). Lunar meteorite olivine and pyroxene compositions are from data acquired by K. Joy (see Figure 8 of Joy et al., Joy et al., 2014 for details; lines trend lines are based on data fits in this figure). Apollo mineral compositions are from a range of literature sources (see Figure 8 of Joy et al., 2014 for references).

Figure 4. Textural similarities between sulphide-bearing fragments in regolith breccia 60016. (a) Left: BSE image of magnetite-troilite-silicate breccia in 60016,83 discussed in this paper (see Figure 2 for full details of image). (b) Right: BSE image of troilite-pentlandite-silicate brecciated region of a crystalline impact melt. This melt breccia intergrowth does not have magnetite as part of the assemblage and is less porous with no clear banding structures compared with the magnetite-bearing fragment shown in (a) and Figure 2.

Figure 5. XANES analysis of Fe-oxide in 60016,83 showing Fe K pre-edge peak of Fe-oxide. The dotted lines show the energy positions of Fe^{2+} and Fe^{3+}. The Fe oxide in 60016,83 is estimated to have a $Fe^{3+}/\Sigma Fe$ ratio of ~0.45, which is close to magnetite.

Figure 6. X-ray diffraction image with simulated pattern for (a) domain 1, (b) domain 2, (c) domain 3 and (d) domain 4. Area of circles shows the calculated intensities of Laue spots. Some diffractions are shown together with their indices.

Figure 7. Phase equilibria for Fe-C-O (grey lines) and Fe-H-O (black lines) over the 300 °C to 1000 °C temperature range using CO_2/CO and H_2O/H_2 ratios calculated from oxygen fugacity values. Fugacity calculations assume pure condensed phases using thermochemical data from Gurvich et al. (1991), Robie and Hemingway (1994), Chase (1998), and Fegley (2013).

Figure 8. Calculated equilibrium phase diagram for Fe-S-O as a function of sulfur fugacity (represented by H_2S/S_2) and oxygen fugacity (represented by H_2O/H_2 and CO_2/CO) at temperatures of (a) 300 °C, (b) 570 °C, and (c) 1000 °C. Fugacity calculations assume pure condensed phases using thermochemical data from Gurvich et al. (1991), Robie and Hemingway (1994), Chase (1998), and Fegley (2013).

Figures

Figure 1

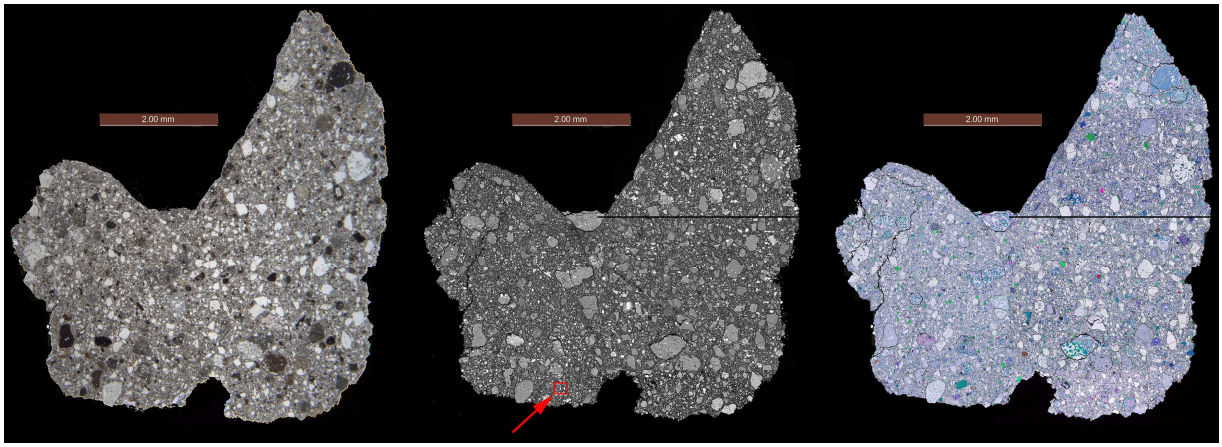

Figure 2

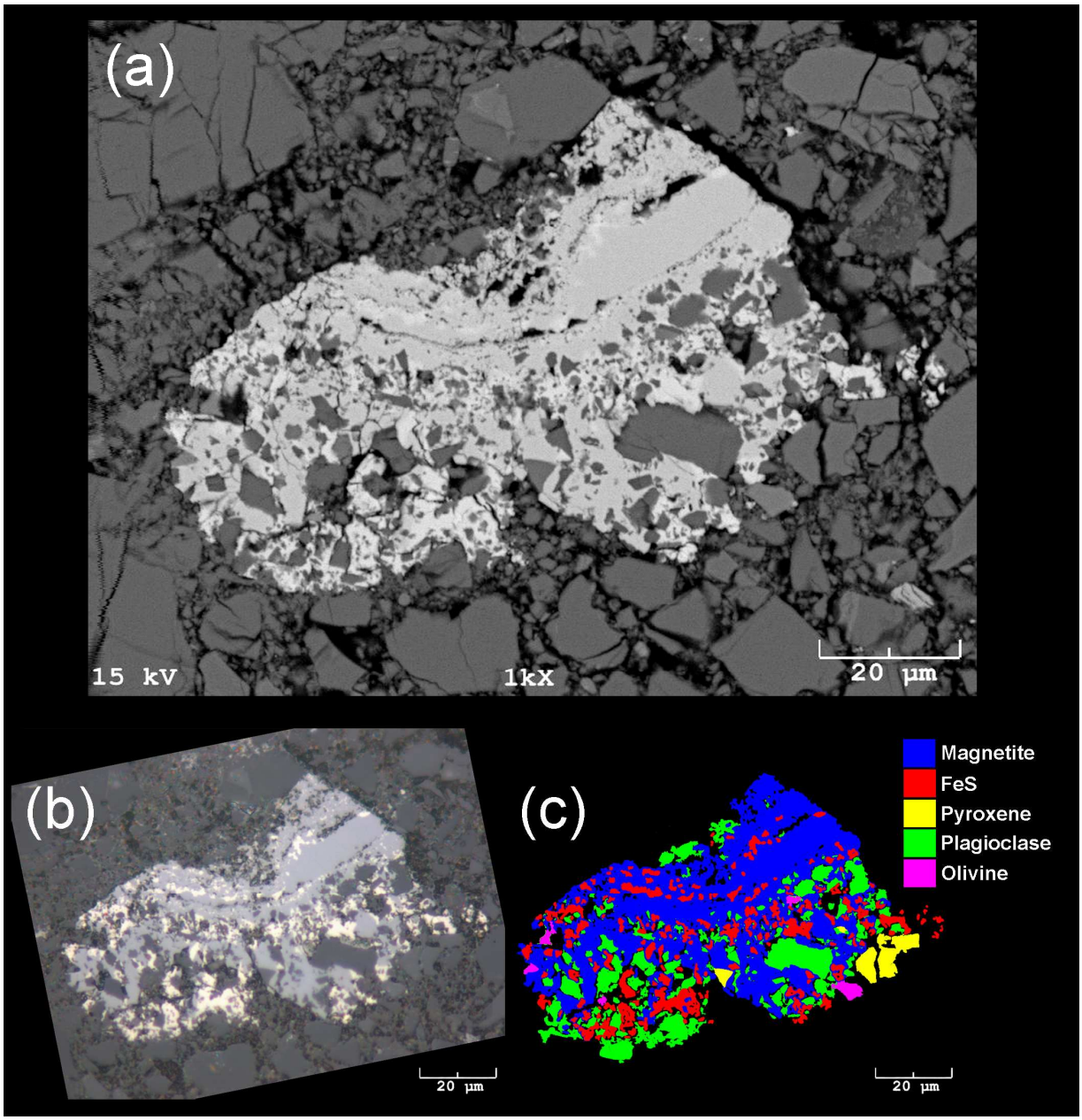
(a)
15 kV
1kX
20 µm
(b)
20 µm
(c)
Magnetite
FeS
Pyroxene
Plagioclase
Olivine
20 µm

Figure 3

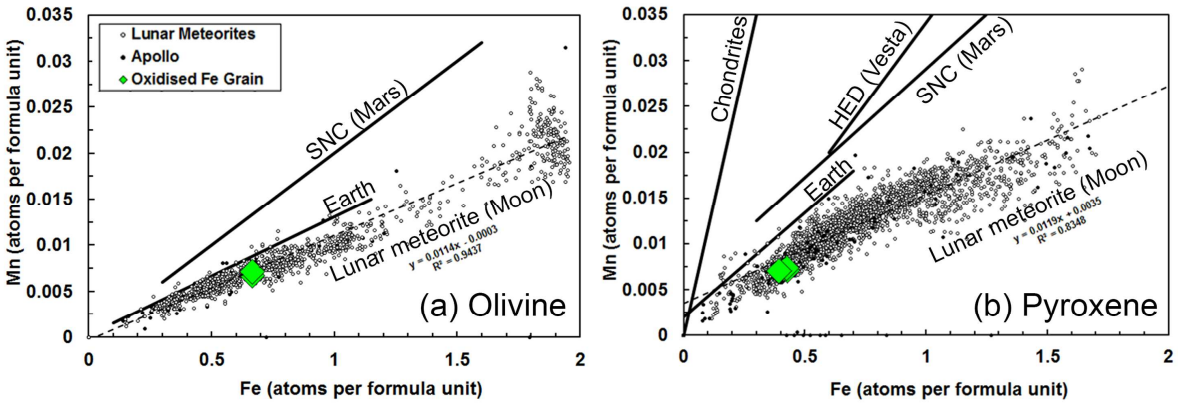

Figure 4

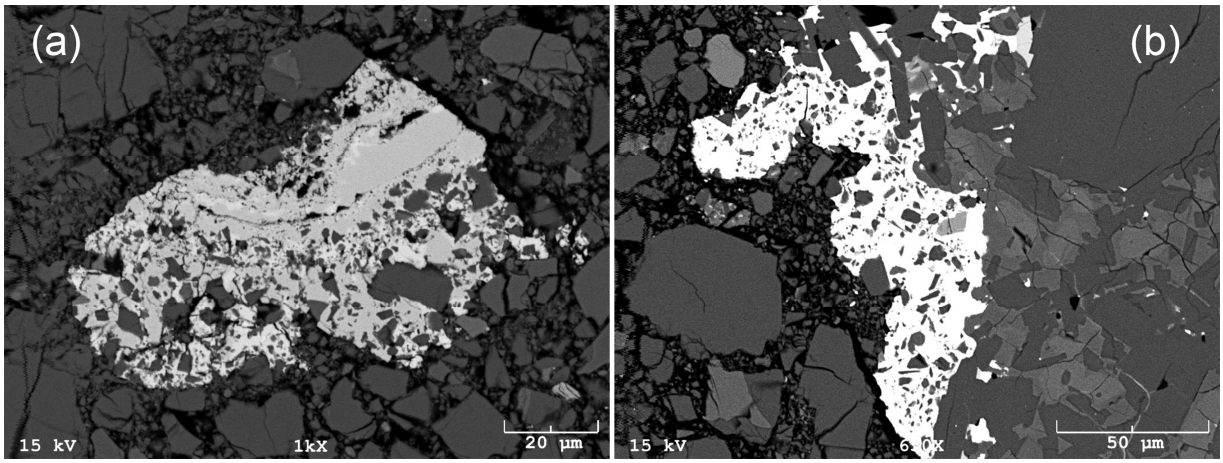

Figure 5

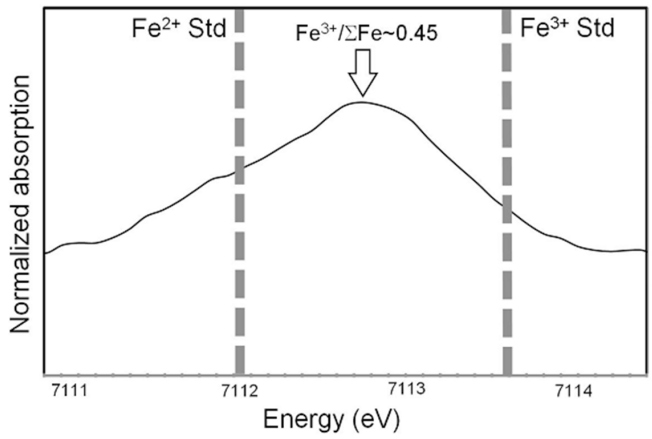

Figure 6

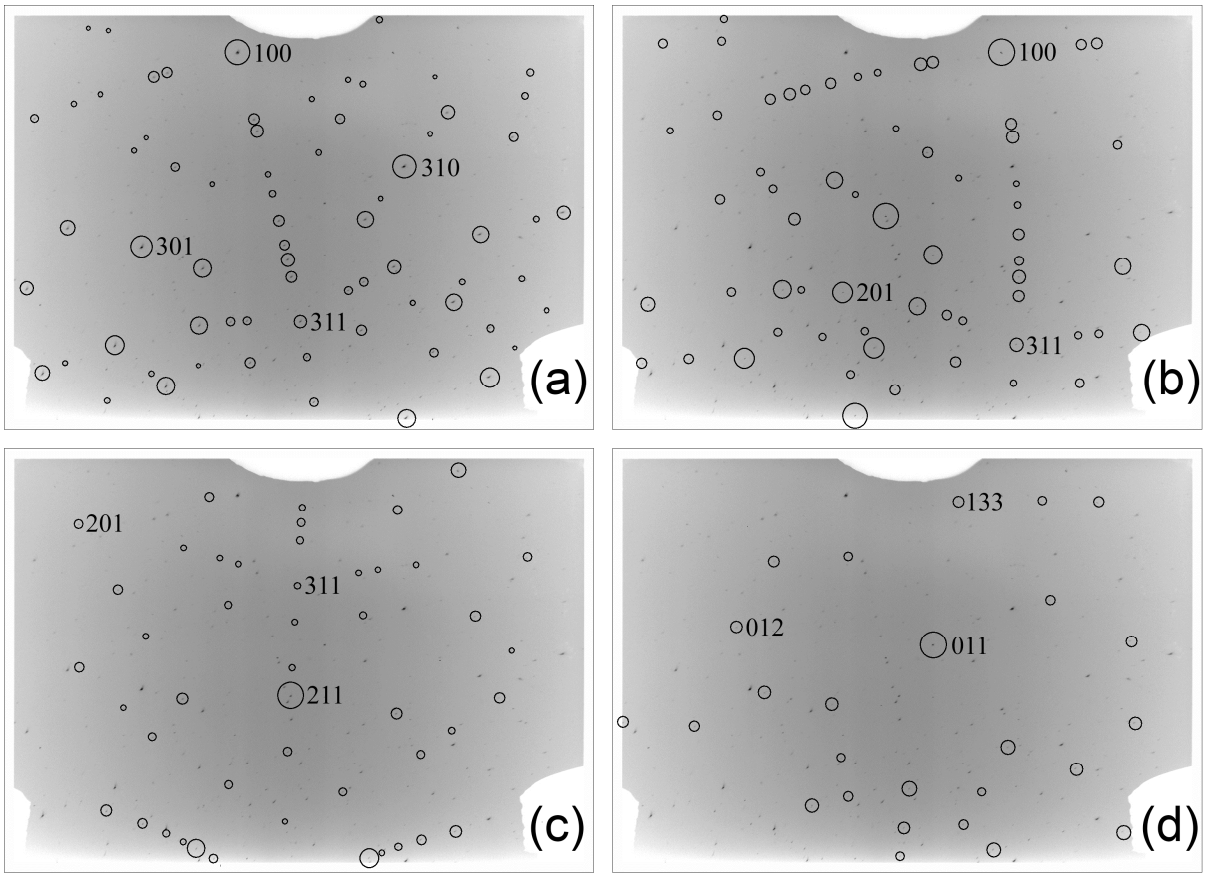

Figure 7

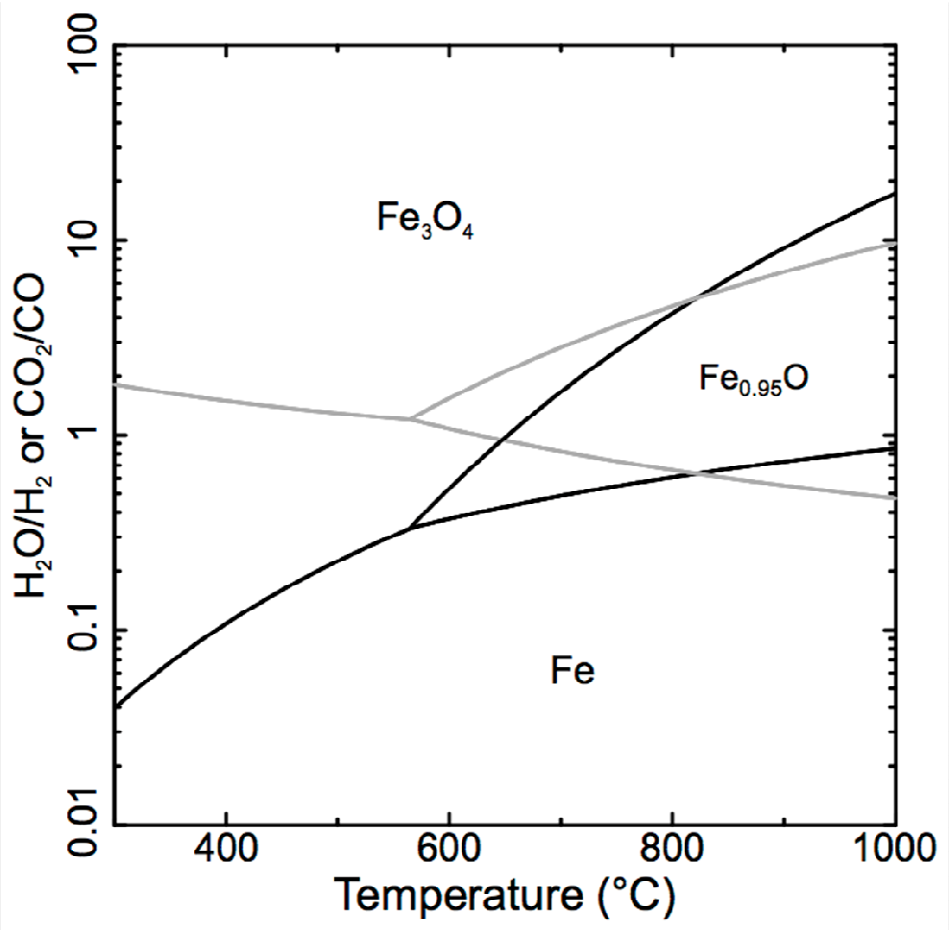
100
10
1
0.1
0.01
H_2O/H_2 or CO_2/CO
Fe_3O_4
$Fe_{0.95}O$
Fe
400
600
800
1000
Temperature (°C)

Figure 8

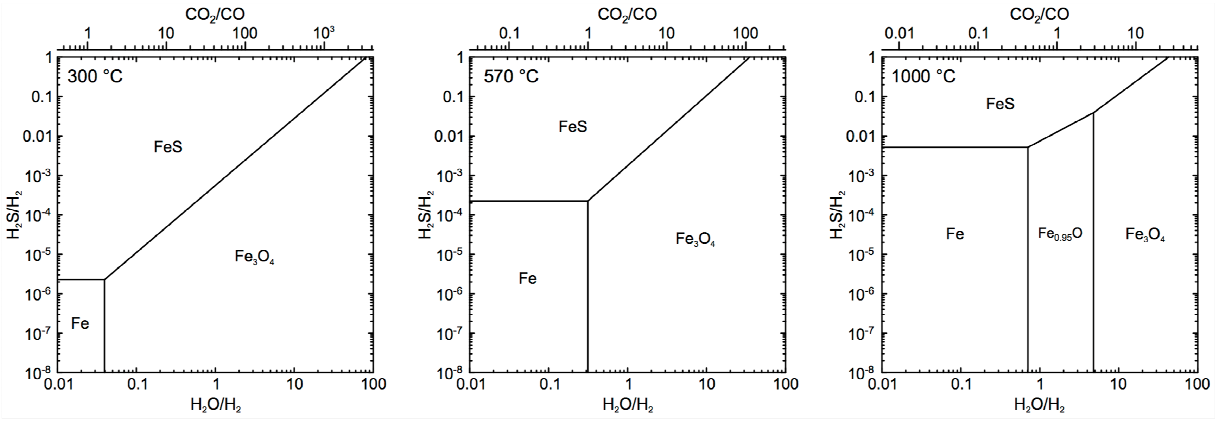
CO2/CO
300 °C
FeS
Fe3O4
Fe
H2S/H2
H2O/H2
570 °C
FeS
Fe3O4
Fe
1000 °C
FeS
Fe
Fe0.95O
Fe3O4

Tables

Table 1. Average composition (10 analyses) of Fe-oxide phase in 60016,83. Fe was standardised using an Fe_3O_4 standard, and only analyses where S was below the detection limits (e.g., <390 ppm) were used in the calculation, to avoid including analyses mixed with surrounding troilite grains. Errors are listed to one standard deviation of the averaged results. TiO_2, Cr_2O_3, MnO, NiO and ZnO wt% concentrations are below the detection limits stated.

	Assuming all Fe as FeO formula	1 st.dev. of multiple (n10) measurements	Assuming $FeO.Fe_2O_3$ formula		Cations (32 oxygens)
SiO_2	0.14	±0.06	0.146	Si	0.045
TiO_2	<0.04		0.000	Ti	0.000
Al_2O_3	0.03	±0.12	0.030	Al	0.011
Cr_2O_3	<0.05		0.000	Cr	0.000
Fe_2O_3			68.702	Fe(iii)	15.899
FeO	92.86	±1.85	31.043	Fe(ii)	7.984
MnO	<0.05		0.000	Mn	0.000
MgO	0.01	±0.05	0.012	Mg	0.006
CaO	0.17	±0.10	0.169	Ca	0.056
NiO	<0.08		0.000	Ni	0.000
ZnO	<0.23		0.000	Zn	0.000
Total	93.22		100.102	**Cations**	24.000

Table 2. Representative composition of other silicate and sulphide mineral phases within magnetite assemblage. b.d. = below detection limits. Errors for silicate minerals are 1 standard deviations (st.dev.) of multiple measurements averaged together. Errors for troilite are based on analytical errors.

	Plagioclase			Pyroxene			Olivine			Troilite	
	Average	1 st.dev.		Average	1 st.dev.		Average	1 st.dev.			1 σ
	(n5)			(n3)			(n2)			(n1)	
SiO_2	43.40	±0.49	**SiO_2**	54.16	±0.57	**SiO_2**	36.49	±0.20	**Si**	0.126	±0.02
TiO2	0.01	±0.01	**TiO2**	0.66	±0.07	**TiO2**	b.d.		**Ti**	<0.04	
Al_2O_3	35.21	±0.41	**Al_2O_3**	1.80	±0.93	**Al_2O_3**	0.31	±0.00	**Cr**	<0.05	
Cr_2O_3	0.02	±0.01	**Cr_2O_3**	0.46	±0.01	**Cr_2O_3**	b.d.		**Fe**	62.89	±1.25
FeO	1.29	±0.32	**FeO**	13.89	±0.69	**FeO**	29.29	±0.04	**Ni**	<0.08	
MnO	0.01	±0.01	**MnO**	0.24	±0.01	**MnO**	0.30	±0.01	**Co**	0.04	±0.02
MgO	0.06	±0.06	**MgO**	27.17	±0.73	**MgO**	32.56	±0.10	**S**	36.16	±0.66
CaO	18.69	±0.22	**CaO**	2.00	±0.36	**CaO**	0.42	±0.06	**P**	<0.03	
Na_2O	0.39	±0.09	**Na_2O**	0.02	±0.03	**Na_2O**	b.d.		**Zn**	<0.19	
K_2O	0.02	±0.01	**K_2O**	b.d.		**K_2O**	b.d.		**Cu**	<0.15	
Total	99.07		***Total***	100.40		***Total***	99.37		***Total***	99.21	
Mg#	8		**Mg#**	78		**Mg#**	66				
An	96.3		**En**	74.6		**FeO/MnO**	97.6				
Al	3.6		**Fs**	21.4							
Or	0.1		**Wo**	4.0							
Stoichiometry	8 oxygen atoms			6 oxygen atoms			4 oxygen atoms				
Si	2.034		**Si**	1.937		**Si**	0.991				
Ti	0.000		**Ti**	0.018		**Ti**	0.000				
Al	1.945		**^{iv}Al**	0.063		**Al**	0.010				
			^{vi}Al	0.013							
Cr	0.001		**Cr**	0.013		**Cr**	0.000				
Fe^{2+}	0.051		**Fe^{2+}**	0.415		**Fe^{2+}**	0.665				
Mn	0.000		**Mn**	0.007		**Mn**	0.007				
Mg	0.004		**Mg**	1.448		**Mg**	1.318				
Ca	0.939		**Ca**	0.077		**Ca**	0.012				
Na	0.035		**Na**	0.001		**Na**	0.000				
K	0.001		**K**	0.000		**K**	0.000				
Total Cations	*5.011*		***Total Cations***	*3.993*		***Total Cations***	*3.004*				
Total Tet. Site	*3.980*		***Total Tet. Site***	*2.000*							

Table 3. Number of XRD analysis observed reflections (refls).

	Back refls.	Transmission refls.	Sub-total
Domain 1	120	69	189
Domain 2	86	53	139
Domain 3	88	45	133
Domain 4	61	40	101
Not assigned	62	76	138
Total	417	283	700